

Brazilian Journal of
Chemical Engineering

**Mathematical Model of the Temperature and the
Concentration Profiles of an Industrial Rotary Kiln Used in
Clinker Production**

Journal:	<i>Brazilian Journal of Chemical Engineering</i>
Manuscript ID	BJCE-2016-0095
Manuscript Type:	Original Article
Date Submitted by the Author:	11-Feb-2016
Complete List of Authors:	Quites Rodrigues, Diulia Caroline; Universidade Federal do Espírito Santo, Soares Jr, Atílio Peixoto ; Fábrica de Cimento Nassau Costa Jr, Esly; Universidade Federal de Minas Gerais da Costa, Andréa; Universidade Federal de Minas Gerais
Keyword:	Mathematical Modelling, Clinker, Rotary Kiln

SCHOLARONE™
Manuscripts

Mathematical Model of the Temperature and the Concentration Profiles of an Industrial Rotary Kiln Used in Clinker Production

D.C.Q. Rodrigues¹, A. P. Soares Jr², E. F. Costa Jr³, A. O. S. Costa³

¹Chemical Engineering Program, Universidade Federal do Espírito Santo – Campus de Alegre CCA/UFES, Alto Universitário, s/n, Caixa Postal 16, CEP: 29500-000 Guararema, Alegre, ES, Brazil. Fax: +55 28 3552-8741

²Fábrica de Cimento Nassau, Cachoeiro de Itapemirim, ES, Brazil.

3Departamento de Engenharia Química, Universidade Federal de Minas Gerais, Antônio Carlos Avenue 6627, Zip Code 31270-901, Belo Horizonte, MG, Brazil

diiliacaroline@hotmail.com, atiliopeixoto@hotmail.com, eslyfcjr@yahoo.com.br,
andreaosc@yahoo.com.br

Abstract

Cement is one of the most used building materials in the world. The process of cement production involves numerous and complex reactions that occur under different temperatures. Thus, there is great interest in the optimisation of cement manufacturing. Clinker production is one of the main steps of cement production and it occurs inside the kiln. In this paper, the dry process of clinker production is analysed in a rotary kiln that operates in counter flow. The main phenomena involved in clinker production is as follows: free residual water evaporation of raw material, decomposition of magnesium carbonate, decarbonation, formation of C_3A and C_4AF , formation of dicalcium silicate, and formation of tricalcium silicate. The main objective of this study was to propose a mathematical model that realistically describes the temperature profile and the concentration of clinker components in a real rotary kiln. In addition, the influence of different speeds of inlet gas and solids in the system was analysed. The mathematical model is composed of partial differential equations. The model was implemented in Mathcad (available at CCA/UFES) and solved using industrial input data. The proposal model is satisfactory to describe the temperature and concentration profiles of a real rotary kiln.

Keywords: Mathematical Modelling, Clinker, Rotary Kiln.

INTRODUCTION

Some of the challenges facing the cement industries are the high energy demand of production, the continuous increase in fuel prices, process complexity and environmental impact (Atmaca and Yumruta, 2014; Gartner and Macphee, 2011; Kaddatz *et al.*, 2013; Mujumdar *et al.*, 2007; Schneider *et al.*, 2011; Tsamatsoulis, 2011). To address these challenges, there is great interest in optimising the cement production process (Copertaro *et al.*, 2015; Utlu *et al.*, 2006).

The best known type of cement is called Portland cement, which is defined as a hydraulic cluster that is basically obtained by grinding a mixture of clinker and gypsum (Copertaro *et al.*, 2015). Thus, one of the main steps of the process for obtaining cement is the synthesis of the clinker (Atsonios *et al.*, 2015; Saidur *et al.*, 2011). Synthesis occurs inside the rotary kiln and involves complex physical (phase changes) and chemical (endothermic and exothermic reactions) processes (Boateng *et al.*, 1996; Lourenço *et al.*, 2013; Saidur *et al.*, 2011; Silva, 2007). The main clinker components are C₃S (3CaO.SiO₂), C₂S (2CaO.SiO₂), C₃A (3CaO.AlO₃) and C₄AF (4CaO.Al₂O₃.Fe₂O₃). The intermediate reactions for obtaining the clinker and their respective heats of reaction are shown in Table 1, and the temperature ranges of the formation of chemicals are shown in Table 2.

Clinker production can be performed in a dry or wet process (Paula, 2009). On one hand, in the dry process, the mixture of agglomerates and aggregates are completely dried and ground to feed the kiln in powder form. On the other hand, in the wet process, the mixture is a mud that is fed into the kiln with approximately 30-40% of moisture (Del Coz Díaz, *et al.*, 2002; Saidur *et al.*, 2011). This paper considers the dry clinker production, which is the most used process in Brazilian production of cement (Kihara *et al.*, 2015).

A rotary kiln in a dry cement production can be divided into five zones (Duarte, 1999; Stadler *et al.*, 2011): heating zone, calcining zone, transition zone, firing zone and cooling zone. The position of the zones along the kiln depends on the temperature and the chemical reactions being performed in the solid (Spang, 1972). The temperature profile along the rotary kiln is generally not directly measured due to the scarcity of sensors that supports its internal operating conditions. Thus, estimating the temperature profile along the kiln is an important object of study.

In a previous work (Spang, 1972), a dynamic model was developed. The model was composed of partial differential equations describing the mass balance and the system power

(Spang, 1972). The model is capable of predicting the concentration and temperature profiles along a rotary kiln operating in counterflow (Spang, 1972). A flame model was also developed to quantify the amount of energy supplied to the system (Spang, 1972). The equations that comprise this model (Equations 1 to 29) are presented in the Appendix. The results qualitatively describe the behaviour of kilns, but the steady state was not reached.

In the present paper, an adaptation of the previous model (Spang, 1972) is implemented to make it more realistic. Using realistic values of the operational properties provided by a Brazilian company, the concentration and temperature profiles of a real rotary kiln used in the industrial production of the clinker is obtained.

WHAT IS THIS ORIGINAL SPANG MODEL
BASED ON? AUTHORS USED TO SUMMARIZE
CALCULATION PROCEDURES IT!

WHY
NOT?

AND WHAT

ABOUT
QUANTITATIVE
BEHAVIOR?

Initially, a modification of the original model (Spang, 1972) was performed to obtain a more realistic description of the temperature and concentration profiles of the clinker components along the rotary kiln.

In the originally proposed model (Spang, 1972) the variation of gas temperature over time was not considered. To improve the description of the process, an adjustment was made in the gas energy balance (Equation 13 of the Appendix), which consisted of adding a term of gas temperature variation into the equation. In this way, Equation 13 was substituted by Equation 30.

$$A_g C_{pg} \rho_g v_g \left(\frac{\partial T_g}{\partial z} \right) = \beta_1 (T_w - T_g) + \beta_2 (T_s - T_g) - C_{pg} \rho_g A_g \left(\frac{\partial T_g}{\partial t} \right) + q_f \quad (30)$$

$$T_g(L, t) = T_{gi}$$

The flame model originally described (Spang, 1972) (Equations 17, 18 and 19 of the Appendix) was replaced by an amount of energy supplied to the kiln by the fuel combustion.

These changes enable the industrial professional to use the model more directly. In this paper, the quantity of energy proposed for the fuel combustion is constant and equal to 326.7 kW/m ($3.9 \times 10^5 \text{ BTU/ft.h}$). This amount, adjusted by trial and error, approaches the values commonly used in industry. Thus, the new proposed model is composed of Equations 1-12, 14-16 and 20-30 as listed in the Appendix.

After adaptations, realistic values of the operational properties of the clinker production as reported by a Brazilian industrial plant were employed in the model. The composition of the raw material used in the industrial production of the clinker is shown in Table 3. The values were normalised in relation to CaO (kg/kg). Other industrial operating properties employed in the model are shown in Table 4. The inner radius of the kiln was estimated to be 1.84 m (6.05 ft), the initial solid temperature, 562°R (312 K), and the initial temperature of the kiln wall, 662°R (367 K). These estimates were performed based on previous data (Spang, 1972) and industrial realities.

The model was solved for different inlet speeds of gas and solid until the final composition of the clinker obtained in the simulation was similar to the actual values obtained in the cement industry (Table 5). The best values for the gas and the solid inlet speeds were 274.32 m/s (-900 ft/hr) and 5.4864 m/s (18 ft/hr), respectively. Next, the temperature and concentration profiles obtained for the rotary kiln were analysed considering these values.

For further analysis, the established inlet speed of gas and solid were varied as -20%, -10%, +10% and +20% to characterise the differences between the systems profiles. Subsequently, the obtained profiles were analysed.

The model was solved using the discretisation method for finite differences. Forty points of discretisation were defined along the length of the rotary kiln. Discretisation of the

points was implemented according to the incoming stream of gas and solids into the kiln (Figure 1). For the discretisation of the equations related to the solids, backward differentiation was used because they are fed into the beginning of the kiln ($z = 0$), and forward differentiation was used in the equations related to the gas because it is fed into the end of the kiln ($z = L$). The ordinary differential equations, functions of time, resulted from the discretisation that were resolved by the numerical integrating method of Runge-Kutta with a variable step for error control, with an established tolerance of 10^{-7} . The model was implemented in Mathcad.

RESULTS AND DISCUSSION

Successive integrations were made in the model equations until the variations between the results were no longer observed, which indicates achievement of the steady state of the rotary kiln. The temperature profiles of the gas, solid, and wall along the kiln's length in continuous operation are presented in Figure 2. As expected, the kiln's temperature increases along its length to a maximum and then decays.

The CaCO_3 concentration profile along the length of the kiln is shown in Figure 3. The profile follows the general pattern of a previous simulation (Spang, 1972). Initially, there is a high concentration of CaCO_3 that decreases along the length of the kiln until it reaches zero.

The water concentration profile along the length of the kiln in steady state is shown in Figure 4. The concentration of molecular water contained in the beginning of the feeding of solids decreases along the kiln until it becomes zero, as expected.

The concentration profiles of C_3S , C_2S , C_3A , C_4AF , and CaO along the length of the kiln in continuous operation are shown in Figure 5. A decreasing behaviour in the

1
2
3
4
5
6
7

concentration of reactants followed by the formation of the clinker components is observed, which is in agreement with the expected.

8
9
10
11
12
13
14
15
16
17
18
19
20
21

The clinker composition simulated by the model and the industrial clinker composition are presented in Table 5. The final concentrations of the clinker components obtained by the model are relatively close to the actual concentrations of the cement industry.

How
close?

The $\text{CaO} \cdot \text{Al}_2\text{O}_3$ and $12\text{CaO} \cdot 7\text{Al}_2\text{O}_3$ elements were not taken into consideration during modelling because they were not considered as part of the main elements of the clinker formation.

22
23
24
25
26
27
28
29
30
31
32
33
34
35
36
37
38
39
40
41
42
43
44
45
46
47
48
49
50
51
52
53
54
55
56
57
58
59
60

Note that the final composition of the clinker widely varies from one industry to another and may vary even between operations of a same kiln because the composition of raw material is not constant, i.e., it may depend of the natural sources. In addition, changes in the operating conditions of a kiln produces variances in the final clinker concentration. An important aspect to highlight is that during the simulation of the actual system, it was not trivial to set values of inlet gas flow and solid flow that together satisfied the required values for the profiles of temperature and clinker concentration.

Why NOT?

The profiles of temperature and clinker concentration obtained by varying the inlet gas speed by -20%, -10%, +10% and +20% are shown in Figures 6 and 7, respectively. The temperature profiles in Figure 6 are very similar, with only slight differences in the shapes of the temperature peaks noticed. In Figure 7, it is observed that C_3A , C_4AF and CaO have similar profiles in all of the proposed systems, whereas C_3S and C_2S have different profiles in each one of them. In general, the increase of the inlet gas speed from -20% to +10% increases the final concentration of C_3S and decreases the final concentration of C_2S . However, with +20% increase of inlet gas speed there is an increase of the final concentration of C_3S and a decrease of C_2S concentration.

AND WHAT
ARE THE
MAIN
CONCLUSIONS
FOR THIS
SENSITIVITY
TEST
DATA ANALYSIS

→ Why?

1
2
3 The temperature and clinker concentration profiles that were obtained by varying the
4 inlet solid speed by -20%, -10%, +10% and +20% are shown in Figures 8 and 9, respectively.
5
6

7 In Figure 8, it is observed that the temperature of the burning zones, which correspond to the
8 highest peak, decrease with the increase of the inlet solid speed. There is also an enlargement
9 of the transition zone that corresponds to the second highest peak. In figure 9, the
10 concentrations of C₃A, C₄AF and CaO along the kiln have relatively similar profiles in all of
11 the proposed systems, whereas C₃S and C₂S have different profiles in each one of them. The
12 increase of the inlet solid speed promotes a later formation of C₃S through the length of the
13 kiln and a decrease in the C₃S final concentration. There is also an increase in the final
14 concentration of C₂S.
15
16
17
18
19
20
21
22
23
24
25
26
27
28
29
30
31
32
33
34
35
36
37
38
39
40
41
42
43
44
45
46
47
48
49
50
51
52
53
54
55
56
57
58
59
60

CONCLUSIONS

31 A mathematical model able to describe the temperature and concentration profiles of
32 the clinker components along a real rotary kiln, in continuous operation, was developed. The
33 mathematical model proposed in this paper does not require advanced computing to be
34 solved, and it is easily adaptable to new industrial realities.

35
36 Variations of the gas and solid inlet speeds by -20%, -10%, +10% and +20% were
37 individuality analysed according to the resulting temperature and concentration profiles of the
38 clinker. These results were obtained via the model in the simulation of the real process. These
39 parameters of operation were chosen because they have a significant influence in the process
40 of cement production, and they can be changed without much modification in the kiln. In
41 addition, these parameters can be used to find new operating conditions for the equipment.

NOMENCLATURE

	Notation	Value	Unit
1	a_n	Proportionality constant for D	0.0538
2	A	#Al ₂ O ₃ /#CaO	
3	A _g	Area of gas at given cross section	ft ²
4	A _i	Initial value of Al ₂ O ₃ /#CaO	#/#CaO
5	A _F	Pre-exponential factor of fuel	5.6 x 10 ¹⁰ 1/h
6	A _s	Area of solid at a given cross section	ft ²
7	A _w	Area of wall at a given cross section	ft ²
8	A _I	Pre-exponential factor of CaCO ₃	1.64 x 10 ³⁵ 1/h
9	A _a	Pre-exponential factor of C ₃ S	4.8x10 ⁸ 1/h
10	A _β	Pre-exponential factor of C ₂ S	1.48x10 ⁹ 1/h
11	A _γ	Pre-exponential factor of C ₃ A	3.0x10 ¹⁰ 1/h
12	A _δ	Pre-exponential factor of C ₄ AF	3.0x10 ¹² 1/h
13	A _ω	Pre-exponential factor of water	7.08x10 ⁷ 1/h
14	C	Calcium Oxide (CaO)	
15	C _F	Normalised amount of available fuel	
16	C _{pg}	Specific heat of gas	0.28 Btu/#°R
17	C _{ps}	Specific heat of solid	0.28 Btu/#°R
18	C _{pw}	Specific heat of wall	0.28 Btu/#°R
19	C ₂ S	2CAO.SiO ₂	
20	C ₃ A	2CAO.Al ₂ O ₃	
21	C ₄ AF	2CAO.Al ₂ O ₃ .FE ₂ O ₃	
22	d ₀	% available oxygen	
23	D ₀	Diffusion coefficient of oxygen	
24	E _F	Activation constant of fuel	2.45x10 ⁴ (Btu/(lbmol))
25	E _I	Activation constant of CaCO ₃	3.46x10 ⁵ (Btu/(lbmol))
26	E _a	Activation constant of C ₃ S	1.10x10 ⁵ (Btu/(lbmol))
27	E _β	Activation constant of C ₂ S	8.3x10 ⁴ (Btu/(lbmol))

1	$E\gamma$	Activation constant of C ₃ A	8.33x10 ⁴	(Btu/(lbmol))
2	$E\delta$	Activation constant of C ₄ AF	7.95x10 ⁴	(Btu/(lbmol))
3	$E\omega$	Activation constant of water	1.807x10 ⁴	(Btu/(lbmol))
4	f ₁	Coefficient of conduction – gas to wall	4	(Btu/(h(ft) ²)°F)
5	f ₂	Coefficient of conduction – solid to gas	4	(Btu/(h(ft) ²)°F)
6	f ₃	Coefficient of conduction – wall to solid	4	(Btu/(h(ft) ²)°F)
7	f ₄	Coefficient of conduction –wall to outside air	0.7	(Btu/(h(ft) ²)°F)
8	F	#Fe ₂ O ₃ / #CaO		
9	F _i	Initial value of #Fe ₂ O ₃ /#CaO	0.0469	#/#CaO
10	G _F	Amount of fuel per hour	53000	#/h
11	h ₀	Fraction of radiation	0.0758	
12	k	Thermal conductivity of the wall	0.9	(Btu/(h(ft) ²)°F)
13	K _f	Radiation rate – fuel		1/h
14	k ₁	Radiation rate - CaCO ₃		1/h
15	k _a	Radiation rate - C ₃ S		1/h
16	k _β	Radiation rate - C ₂ S		1/h
17	k _γ	Radiation rate - C ₃ A		1/h
18	k _δ	Radiation rate - C ₄ AF		1/h
19	k _ω	Radiation rate – water		1/h
20	L	Total length of the kiln	400	ft
21	M	Depending on the subscript molecular weight of the chemicals		
22	^M C ₁	Molecular weight of Carbon (C)		lb
23	P	Pressure		Btu/ft ²
24	p	Angle subtended by the surface of solid	3π/2	Radians
25	q _c	Heat generated by the chemical reactions		(Btu/(ft ³ h))
26	(q _F)	Heat generated by the fuel		(Btu/(ft h))
27	R	Ideal Gas constant	1.987	Btu lbmol ⁻¹ R ⁻¹
28	Q	Heat generated or moving into a region		

1	r_F	Particle size of the fuel	10^{-2}	ft
2	r_1	Inside radius of the kiln	5	ft
3	r_2	Outside radius of the kiln	6	ft
4	r_3	Ratio of heat transfer in the chain section	5	ft
5	$R\omega$	Reaction rate of water		[h^{-1}]
6	S	#SiO ₂ /#CAO		
7	S_i	Initial value of #SiO ₂ /#CAO	0.3398	#/#CAO
8	T_a	Temperature outside the kiln	561.7	°R
9	T_g	Temperature of the solid		°R
10	T_{gi}	Input temperature of the gas	1700	°R
11	T_s	Temperature of the solid		°R
12	T_{si}	Initial temperature of the solid	562	°R
13	T_w	Temperature of the wall		°R
14	v_g	Velocity of the gas	40000	ft/h
15	v_s	Velocity of the solid	-150	ft/h
16	z	Distance along the kiln		ft
17	α	#C ₃ S/#CAO		
18	β	#C ₂ S/#CAO		
19	$\beta_1, \beta_2, \beta_3,$	Heat transfer coefficient		(Btu/(h°R))
20	β_4			
21	γ	#C ₃ A/#CaO		
22	δ	#C ₄ AF/#CaO		
23	ΔH_ξ	Heat of reaction - CaCO ₃	1275	Btu/#CaCO ₃
24	ΔH_F	Heat of reaction – fuel	-14000	Btu/#CaCO ₃
25	ΔH_α	Heat of reaction - C ₃ S	11	Btu/#C ₃ S
26	ΔH_β	Heat of reaction - C ₂ S	-381	Btu/#C ₂ S
27	ΔH_ω	Heat of reaction – water	970	Btu/#água
28	ε_g	Radiation coefficient – gas	0.273	
29	ε_s	Radiation coefficient – solid	0.500	
30	ε_w	Radiation coefficient – wall	0.751	

1	ξ	#CaCO ₃ /#CaO		
2	ξ_i	Initial value of #CaCO ₃ /#CaO at the input	1.784	#/#CaO
3	ρ_F	Density of the fuel		#/#ft ³
4	ρ_g	Density of the gas	0.05	#/#ft ³
5	ρ_s	Density of the solid	56	#/#ft ³
6	ρ_w	Density of the wall	112	#/#ft ³
7	Ψ	#CO ₂ /#CaO		
8	ω	#water/#CaO		
9	ω_i	Initial value of #água/#CaO	0.0649	#/#CaO
10				
11				
12				
13				
14				
15				
16				
17				
18				
19				
20				
21				
22				
23				
24				
25				
26				
27				
28				
29		The authors thank CNPq for the DTI productivity grant and FAPES for the		
30				
31		scholarship Pesquisador Capixaba.		
32				
33				
34				
35				
36				
37				
38				
39				
40				
41				
42				
43				
44				
45				
46				
47				
48				
49				
50				
51				
52				
53				
54				
55				
56				
57				
58				
59				
60				

ACKNOWLEDGMENTS

APPENDIX

Material balance equations:

Water:
$$\left\{ \begin{array}{l} \frac{\partial \omega}{\partial t} = -R_\omega - v_s \frac{\partial \omega}{\partial z}, \\ \omega(0, t) = \omega_i K_\omega \omega > 0.1 \end{array} \right. \quad (1)$$

CO₂:

$$\frac{\partial \Psi}{\partial t} = \frac{A_s \rho_s M_\Psi}{A_g \rho_g M_C} k_1 \xi - v_g \frac{\partial \Psi}{\partial z}, \quad \Psi(L, t) = 0 \quad (2)$$

CaCO₃:

$$\frac{\partial \xi}{\partial t} = -k_1 \xi \frac{M_\xi}{M_C} - v_s \frac{\partial \xi}{\partial z}, \quad \xi(0, t) = \xi_i \quad (3)$$

C₃S:

$$\frac{\partial \alpha}{\partial t} = \frac{M_\alpha}{M_C} k_\alpha (C) \beta - v_s \frac{\partial \alpha}{\partial z}, \quad \alpha(0, t) = 0 \quad (4)$$

C₂S:

$$\frac{\partial \beta}{\partial t} = \frac{M\beta}{2M_C} k_\beta (C^2) S - \frac{M\beta}{M_C} k_\alpha (C) \beta - v_s \frac{\partial \beta}{\partial z}, \quad \beta(0, t) = 0 \quad (5)$$

C₃A:

$$\frac{\partial \gamma}{\partial t} = \frac{M\gamma}{3M_C} k_\gamma (C^3) A - v_s \frac{\partial \gamma}{\partial z}, \quad \gamma(0, t) = 0 \quad (6)$$

C₄AF:

$$\frac{\partial \delta}{\partial t} = \frac{M\delta}{4M_C} k_\delta (C^4) AF - v_s \frac{\partial \delta}{\partial z}, \quad \delta(0, t) = 0 \quad (7)$$

Fe₂O₃:

$$\frac{\partial F}{\partial t} = - \frac{M_F}{4M_C} k_\delta (C^4) AF - v_s \frac{\partial F}{\partial z}, \quad F(0, t) = F_i \quad (8)$$

Al₂O₃:

$$\frac{\partial A}{\partial t} = - \frac{M_A}{4M_C} k_\delta (C^4) AF - \frac{M_A}{4M_C} k_\gamma (C^3) A - v_s \frac{\partial A}{\partial z}, \quad A(0, t) = A_i \quad (9)$$

SiO₂:

$$\frac{\partial S}{\partial t} = - \frac{M_S}{2M_C} k_\beta S (C^2) - v_s \frac{\partial S}{\partial z}, \quad S(0, t) = S_i \quad (10)$$

CaO:

$$\frac{\partial C}{\partial t} = -k_1 \xi - k_\alpha C \beta - k_\beta S (C^2) - k_\gamma C^3 A - k_\delta C^4 AF - v_s \frac{\partial C}{\partial z}, \quad C(0, t) = 0 \quad (11)$$

Fuel (coal/oil):

$$\frac{\partial C_F}{\partial z} = \frac{1}{\rho_g v_g} \left[\frac{\Psi^M C_1 (PM_a)^2}{\rho_F M_{O_2} (RT_g)^2} \right] k_F d_0 C_F, \quad C_F(L, t) = C_{F_i} \quad (12)$$

Thermodynamic energy balance equations:

Gas:

$$A_g C_{pg} \rho_g v_g \left(\frac{\partial T_g}{\partial z} \right) = \beta_1 (T_w - T_g) + \beta_2 (T_s - T_g) + q_f \quad (13)$$

$$T_g(L, t) = T_{gi}$$

Solid:

$$A_s C_{ps} \rho_s v_s \left(\frac{\partial T_s}{\partial z} \right) = \beta_2 (T_g - T_s) + \beta_3 (T_w - T_s) - C_{ps} \rho_s A_s \left(\frac{\partial T_s}{\partial t} \right) + A_s q_c \quad (14)$$

$$T_s(0, T) = T_{si}$$

1
2
3 Kiln wall:

$$A_w C_{pw} \rho_w \left(\frac{\partial T_w}{\partial t} \right) = \beta_1 (T_g - T_w) + \beta_3 (T_s - T_w) + \beta_4 (T_a - T_w) \quad (15)$$

4
5
6
7 Heat of reaction:

$$q_c = \frac{\rho_s}{(1+A_i+F_i+S_i)} [-\Delta H_\xi k_1 \xi - \Delta H_\omega R_\omega - \Delta H_\beta k_\beta S(C^2) - \Delta H_\alpha k_\alpha C \beta] \quad (16)$$

8
9 Flame model:

$$q_f = \frac{G_f (-\Delta H_F)}{(p_g v_g)} \left[\frac{\Psi^M C_1 (PM_a)^2}{\rho_s M_{O_2} (RT_g)^2} \right] k_F d_0 C_F \quad (17)$$

$$d_0 = 1 - \frac{k_F}{\left(\frac{D_0^3}{r_F^2} \right) + k_F} \quad (18)$$

$$D_0 = a_0 T_g^{\frac{3}{2}} \quad (19)$$

24
25 Reaction rate coefficient:

$$k_i = A_i \exp \left(\frac{-E_i}{RT_i} \right) \quad (20)$$

26
27 i = 1, $\underline{\alpha}$, $\underline{\beta}$, $\underline{\gamma}$, $\underline{\delta}$, ω

$$k_F = \frac{3}{r_F} A_F \exp \left(\frac{-E_F}{RT_g} \right) \quad (21)$$

33
34 Coefficient of heat transfer:

$$\beta_1 = r_1 p [f_1 + 1.73 \times 10^{-9} (1 - h_0) \varepsilon_g \varepsilon_w (T_g^2 + T_w^2) (T_g + T_w)] \quad (22)$$

$$\beta_2 = 2r_1 \sin \left(\frac{p}{2} \right) [f_2 + 1.73 \times 10^{-9} \varepsilon_g \varepsilon_s (T_g^2 + T_s^2) (T_g + T_s)] \quad (23)$$

$$\beta_3 = r_1 (2\pi - p) [f_3 + 1.73 \times 10^{-9} h_0 \varepsilon_w \varepsilon_s (T_w^2 + T_s^2) (T_w + T_s)] \quad (24)$$

$$\beta_4 = 2\pi f_4 r_2 \quad (25)$$

$$h = 1 + \frac{2h_0 \sin(\frac{p}{2})}{2\pi - p} \quad (26)$$

46
47 Area coefficient:

$$A_g = \frac{r_1^2}{2} (p - \sin p) \quad (27)$$

$$A_s = \frac{r_1^2}{2} (2\pi - p + \sin p) \quad (28)$$

$$A_w = 2\pi (r_2^2 - r_1^2) \quad (29)$$

1
2
3
4
5 REFERENCES
6
7
8
9

10 Atmaca, A. and Yumruta, R., Analysis of the parameters affecting energy consumption of a
11 rotary kiln in cement industry. Applied Thermal Engineering, 66, 435- 444 (2014).
12
13 Gartner, E. M. and Macphee, D. E., A physico-chemical basis for novel cementitious binders.
14 Cement and Concrete Research, 41, 736-749 (2011).
15 Kaddatz, K. T., Rasul, M. G. and Azad, R., Alternative fuels for use in cement kilns: process
16 impact modelling. Procedia Engineering, 56, 413-420 (2013).
17
18 Mujumdar, K. S. B., Ganesh, K. V., Kulkarni, S. B. and Ranade, V. V., Rotary Cement
19 Kiln Simulator (RoCKS): Integrated modeling of pre-heater, calciner, kiln and clinker
20 cooler. Chemical Engineering Science, 69, 2590-2607 (2007).
21
22 Schneider, M., Romer, M., Tschudin, M. and Bolio, H., Sustainable cement production -
23 present and future. Cement and Concrete Research, 41, 642-650 (2011).
24
25 Tsamatsoulis, D. C., Optimizing the control system of cement milling: process modeling and
26 controller tuning based on loop shaping procedures and process simulations. Brazilian
27 Journal of Chemical Engineering, 31, 155-170 (2014).
28
29 Utlu, Z., Sogut, Z., Hepbasli, A. and Oktay, Z., Energy and exergy analyses of a raw mill in a
30 cement production. Applied Thermal Engineerin, 26, 2479-2489 (2006).
31
32 Copertaro, E., Chiariotti, P., Estupinan, D., Alvaro, A., Paone, N., Peters, B. and Revel, G.
33 M., A discrete-continuous approach to describe CaCO₃ decarbonation in non-steady
34 thermal conditions. Powder Technology, 275, 131-138 (2015).
35
36 Atsonios, K., Grammelis, P., Antiohos, S. K., Nikolopoulos, N. and Kakaras, E., Integration
37 of calcium looping technology in existing cement plant for CO₂ capture: Process
38 modelling and technical considerations. Fuel, 153, 210-223 (2015).
39
40
41
42
43
44
45
46
47
48
49
50
51
52
53
54
55
56
57
58
59
60

ALPHA BETICAL (OR
NUMERICAL) OR DE!!!

- Saidur, R., Hossaina, M. S., Islama, M. R., Fayaz, H. and Mohammed, H. A., A review on kiln system modeling. Renewable and Sustainable Energy Reviews, 15, 2487-2500 (2011).
- Boateng, A. A. and Barr, P. V., A thermal model for the rotary kiln including heat transfer within the bed. Pergamon, 39, 2131-2147 (1996).
- Silva, M. C. C., Relações entre microestrutura, composição, resistência à ruptura e moabilidade de clíqueres de cimento Portland. Masters Dissertation, Brazil: COPPE/Universidade Federal do Rio de Janeiro (2007).
- Lourenço, R. R., Angélica, R. S. and Rodrigues, J. A., Preparation of refractory calcium aluminate cement using the sonochemical process. Material Research, 16, 731-739 (2013).
- Paula, L. G., Análise termoeconômica do processo de produção de cimento Portland com co-processamento de misturas de resíduos. Masters Dissertation, Brazil: Universidade Federal de Itajubá (2009).
- Smith, J. M., Van Ness, H. C. and Abbott, M. M., Introdução à termodinâmica da Engenharia Química. Ed. LTC, Rio de Janeiro – RJ (2007).
- Del Coz Díaz, J. J., Mazóna, F., Rodrigues, N., García, D. and Suárez, F. J., Design and finite element analysis of a wet cycle cement rotary kiln. Finite Elements in Analysis and Design, 39, 17-42 (2002).
- Kihara, Y. and Visedo, G., A indústria do cimento e o desenvolvimento do Brasil. Associação Brasileira de Cimento Portland, Maio de 2014. Available from: <<http://www.abcp.org.br/conteudo/imprensa/a-industria-do-cimento-e-o-desenvolvimento-do-brasil#.VQLvgo7F9NP>>. Access in: 19/05/2015.

1
2
3 Stadler, K. S., Poland, J. and Gallestey, E., Model predictive control of a rotary cement kiln.
4
5 Control Engineering Practice, 19, 1-9 (2011).
6

7 Spang, H. A., A dynamic model of a cement kiln. Pergamon Press, 8, 309-323 (1972).
8
9

10 Duarte, V. C. Estudo da transferência de calor em fornos rotativos da indústria de cimento,
11
12 utilizando o Método de Elementos Finitos. Masters Dissertation, Brazil: Universidade
13
14 Federal de Itajubá, UNIFEI (1999).
15
16
17
18
19
20
21
22
23
24
25
26
27
28
29
30
31
32
33
34
35
36
37
38
39
40
41
42
43
44
45
46
47
48
49
50
51
52
53
54
55
56
57
58
59
60

Table 1 - Chemical reactions of the clinker production process (Paula, 2009; Smith *et al.*, 2007)

Clinkerisation step	Chemical Reaction	Reaction heat (kJ/kg)
Evaporation of residual free water and water as a result of the clay combination	$H_2O(l) \rightarrow H_2O(v)$	+2443 (a 25°C)
Calcination	$CaCO_3(s) \leftrightarrow CaO(s) + CO_2(g)$	+1766 (a 20°C)
Magnesium carbonate decomposition	$MgCO_3(s) \rightarrow MgO(s) + CO_2(g)$	+1188 (a 20°C)
Formation of the liquid phase	$3CaO(s) + Al_2O_3(s) \rightarrow 3CaO.Al_2O_3(s) (C_3A)$ $4CaO(s) + Al_2O_3(s) + Fe_2O_3(s) \rightarrow 4CaO.Al_2O_3. Fe_2O_3(s) (C_4AF)$	-15 (a 20°C) -84 (a 20°C)
Formation of silicate dicalcium	$2CaO(s) + SiO_2(s) \rightarrow 2CaO. SiO_2(s) (C_2S)$	-717 (a 20°C)
Formation of tricalcium silicate	$3CaO(s) + SiO_2(s) \rightarrow 3CaO. SiO_2(s) (C_3S)$	-528 (a 20°C)

Table 2 – Temperatures of the chemical reactions of clinker production (Paula, 2009)

Temperature	Chemical Reaction
Above 800°C	Start of the CaO manufacturing process
Between 800°C and 1200°C	Formation of C ₂ S
Between 1095°C e 1205°C	Formation of C ₃ A and C ₄ AF
Between 1260°C e 1455°C	Formation of C ₃ S from C ₂ S Crystallisation of C ₃ A and the C ₄ AF liquid phase C ₂ S and C ₃ S silicate practically remain unchanged both in form and composition
Between 1455°C e 1300°C	

Table 3 - Input composition of the raw material in the rotary kiln reported by industry

Chemical Species	Normalised Composition in relation to CaO (kg/kg)
CaCO ₃	1.6666
SiO ₂	0.4849
Al ₂ O ₃	0.1133
Fe ₂ O ₃	0.0651
H ₂ O	0.0117

Table 1 - Rotary kiln data reported by industry

Variables	American Units	International System
Inlet gas temperature	1391.67 °R	773.15 K
Radio of the kiln (r)	7.00 ft	2.15 m
Length of the kiln	295.28 ft	90.00 m
Outside radius (r2)	2.148 m	7.05 ft

Table 5 - Comparison of the results obtained by the model and the industrial composition of the clinker.

Chemical Species	Industrial Composition of the Clinker (mol/mol)	Simulated Composition of the Clinker (mol/mol)
3CaO.SiO ₂	0.5600	0.4630
2CaO.SiO ₂	0.2215	0.3074
CaO.Al ₂ O ₃	0.0848	-
12CaO.7Al ₂ O ₃	0.0087	-
3CaO.Al ₂ O ₃	0.0816	0.1706
4CaO.Al ₂ O ₃ .Fe ₂ O ₃	0.0433	0.0589
CaO	0.0000	0.0000
TOTAL	0.9999	0.9999

FIGURE CAPTION

Figure 1: Volume control used in the mathematical modelling of the rotary kiln (adapted from Spang (1972)).

Figure 2: Temperature profiles of the gas, the solid and the industrial rotary kiln's wall at steady state.

Figure 3: Concentration profiles of CaCO₃ in the industrial rotary kiln at steady state.

Figure 4: Concentration profiles of water in the industrial rotary kiln at steady state.

Figure 5: Concentration profiles of C₃S, C₂S, C₃A, C₄AF and CaO in the industrial rotary kiln at steady state.

Figure 6: Temperature profiles of the gas, the solid, and the wall of the industrial rotary kiln at steady state. (a) -20% of inlet gas speed; (b) -10% of inlet gas speed; (c) +10% of inlet gas speed; (d) +20% of inlet gas speed.

Figure 7: Concentration profiles of C₃S, C₂S, C₃A, C₄AF and CaO in the industrial rotary kiln at steady state. (a) -20% of inlet solid speed; (b) -10% of inlet solid speed; (c) +10% of inlet solid speed; (d) +20% of inlet solid speed.

Figure 8: Temperature profiles of the gas, the solid, and the wall of the industrial rotary kiln at steady state. (a) -20% of inlet solid speed; (b)-10% of inlet solid speed; (c) +10% of inlet solid speed; (d) +20% of inlet solid speed.

Figure 9: Concentration profiles of C₃S, C₂S, C₃A, C₄AF and CaO in the industrial rotary kiln at steady state. (a) -20% of inlet gas speed; (b) -10% of inlet gas speed; (c) +10% of inlet gas speed; (d) +20% of inlet gas speed.

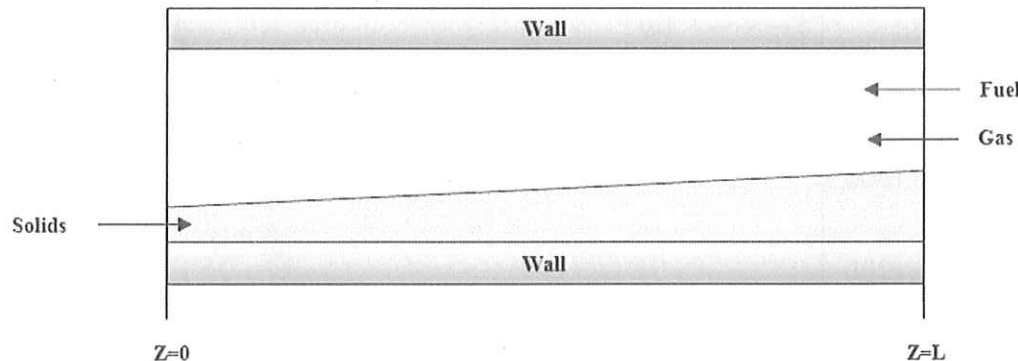
FIGURES

Figure 1

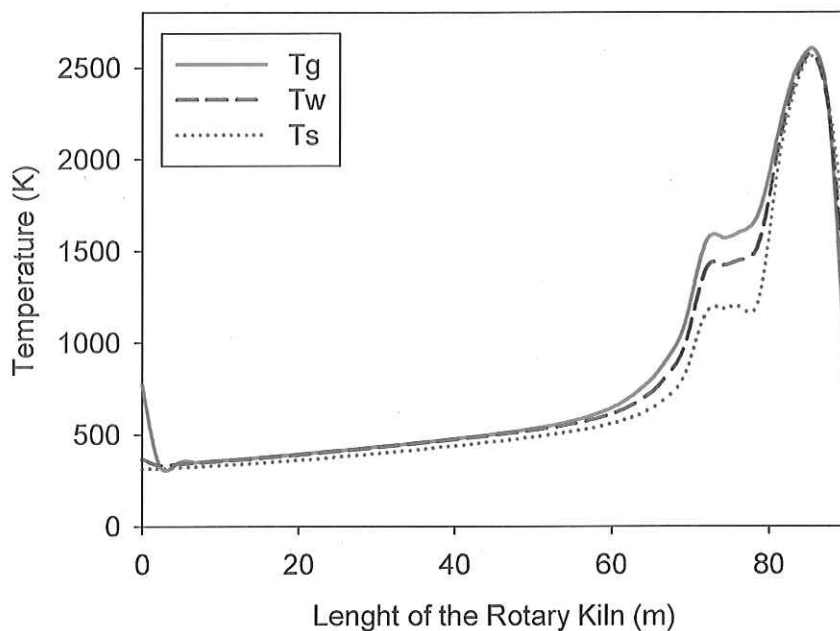
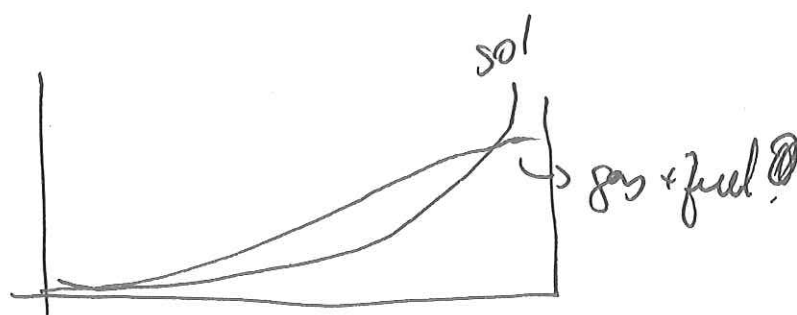


Figure 2

Is the axis direction correct? If fuel + gas system is counterflow of solid, shouldn't the ~~no~~ Dist. $\times T$ present @ 2 peaks?



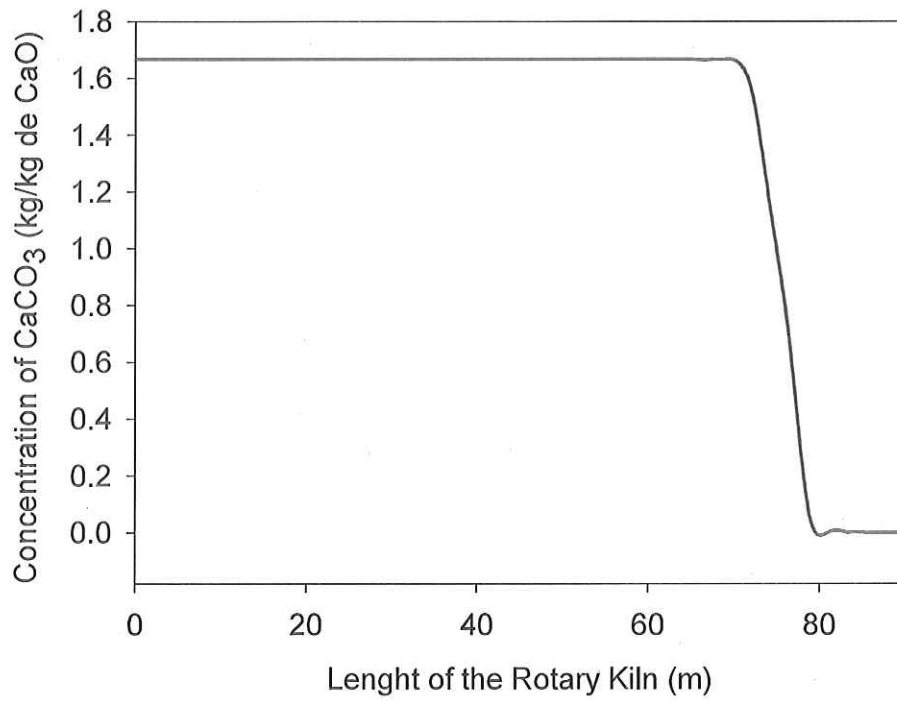


Figure 3

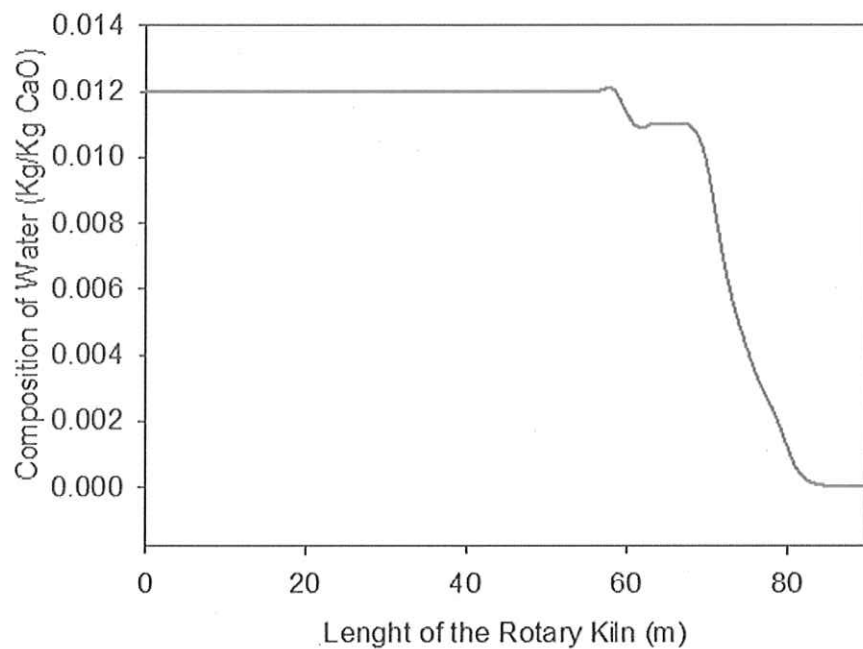


Figure 4

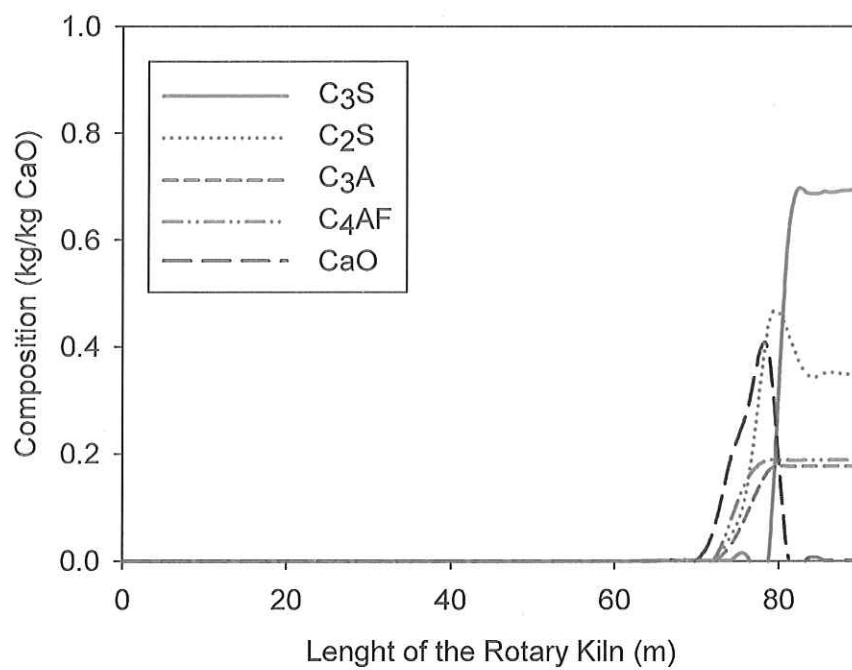


Figure 5

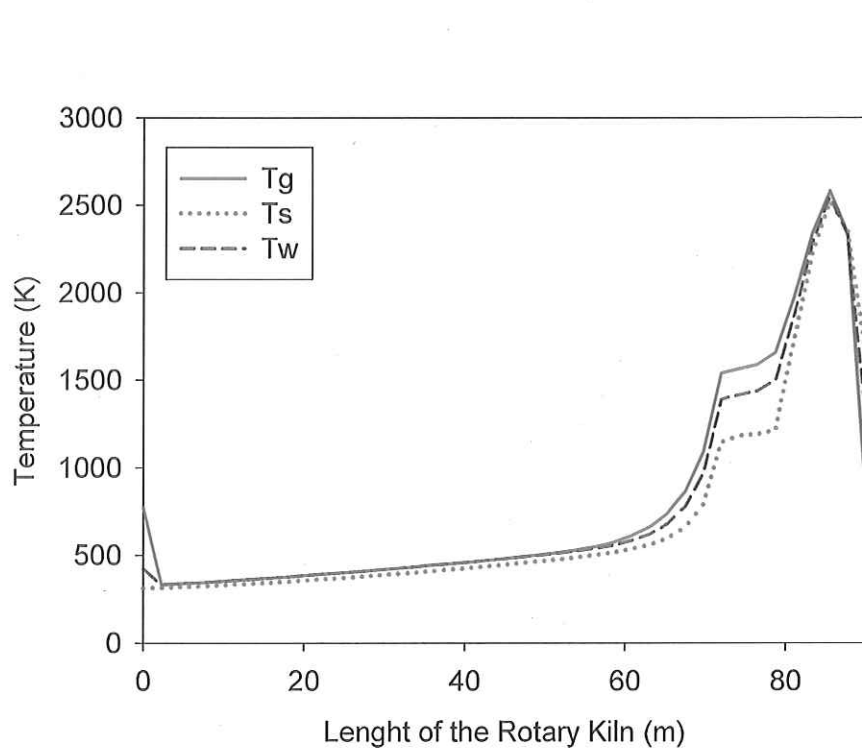


Figure 6 (a)

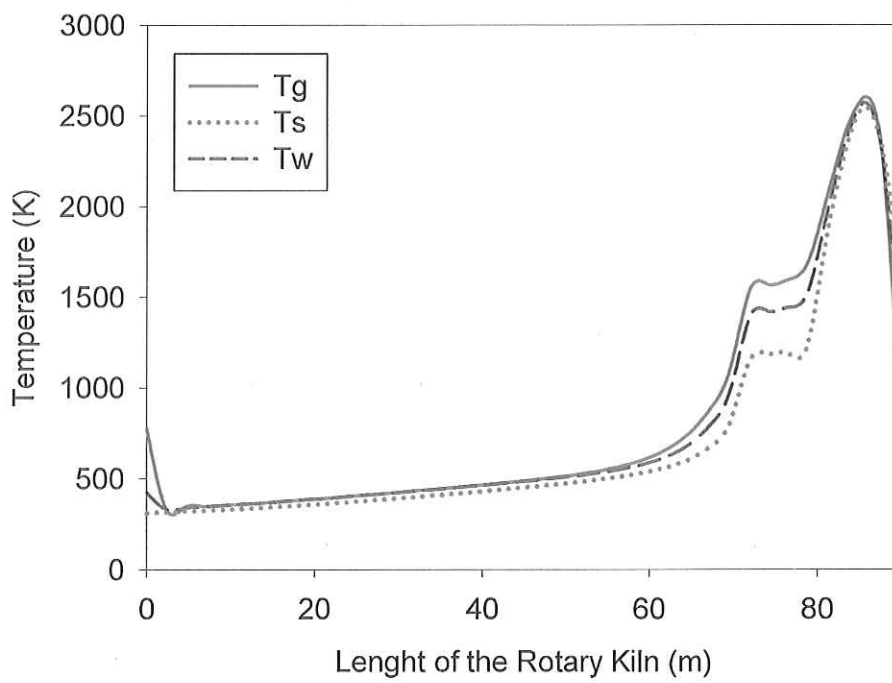


Figure 6 (b)

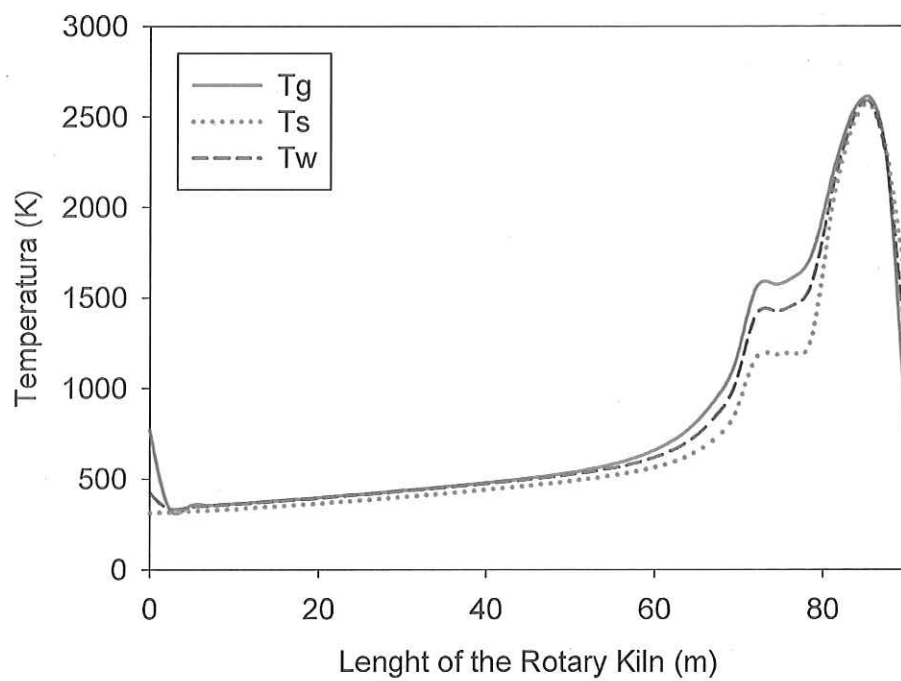


Figure 6 (c)

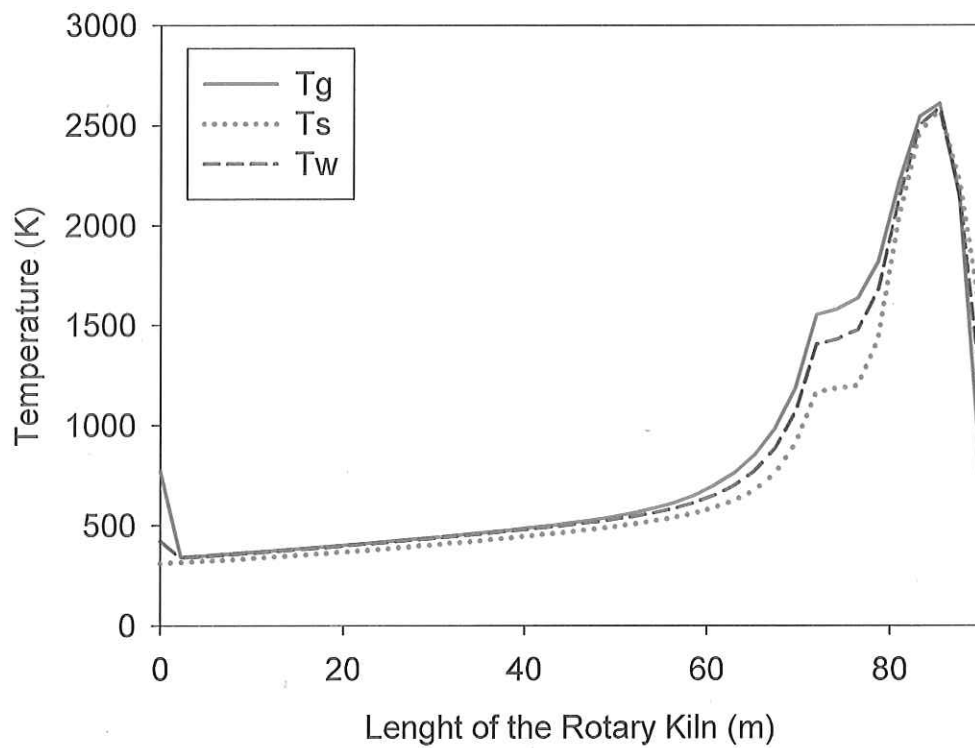


Figure 6 (d)

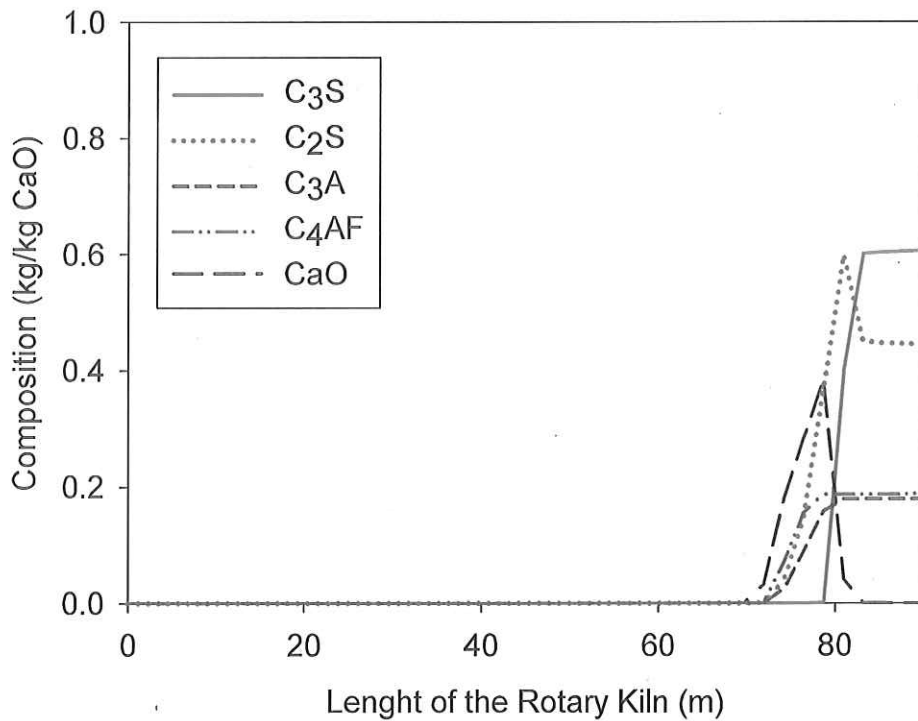


Figure 7 (a)

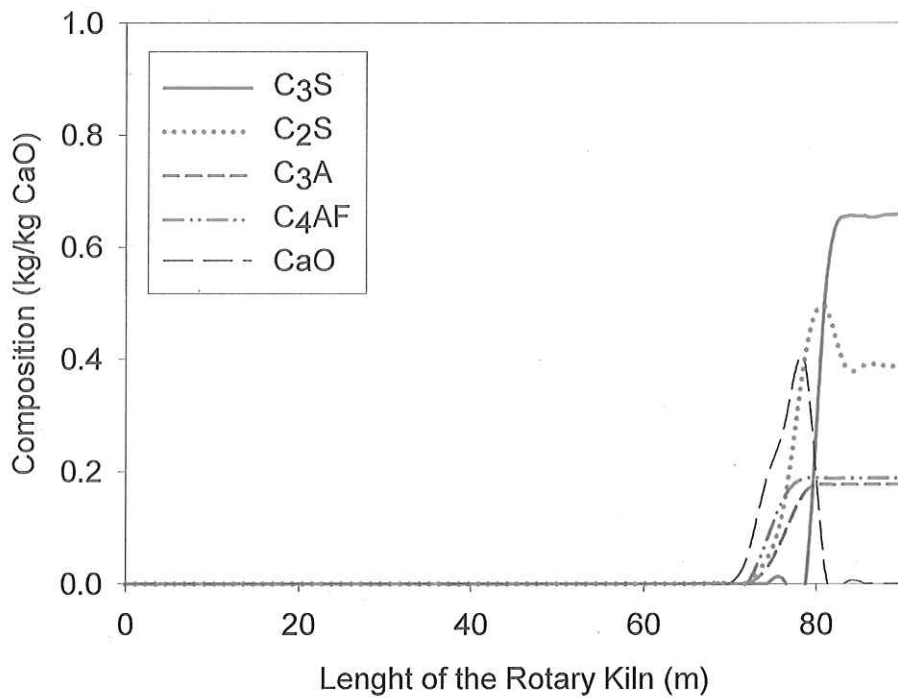


Figure 7 (b)

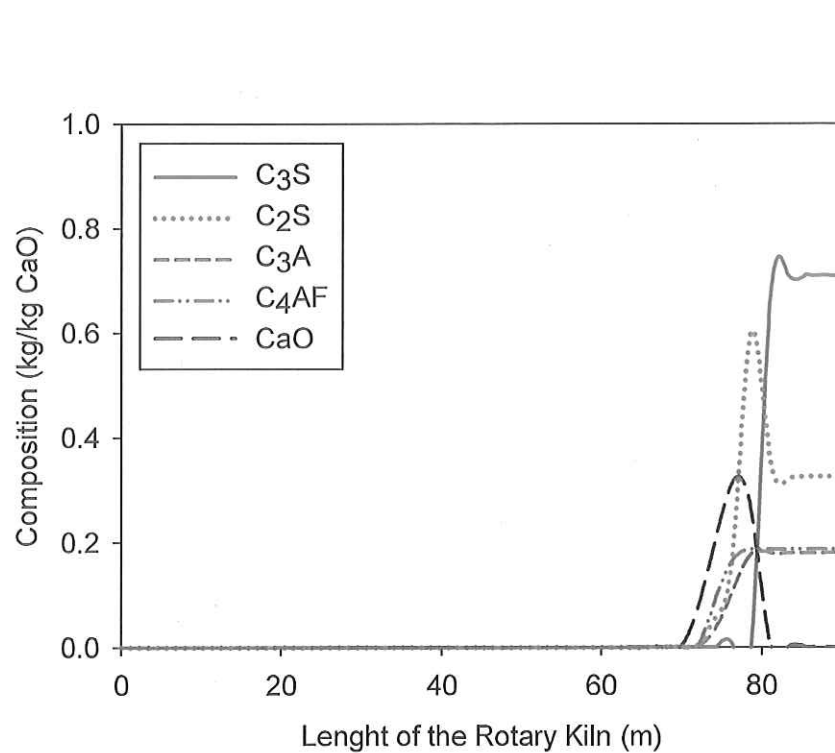


Figure 7 (c)

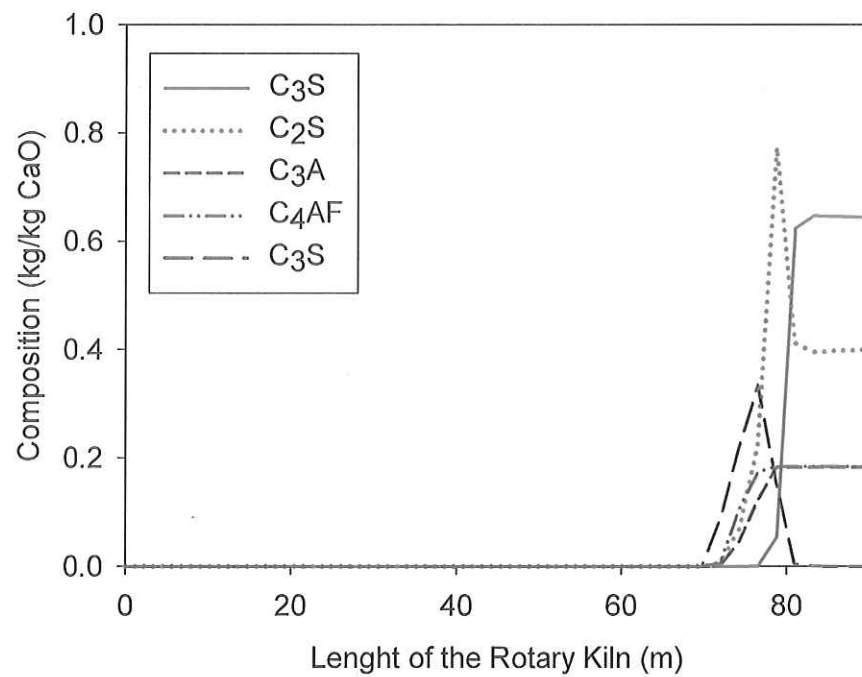


Figure 7 (d)

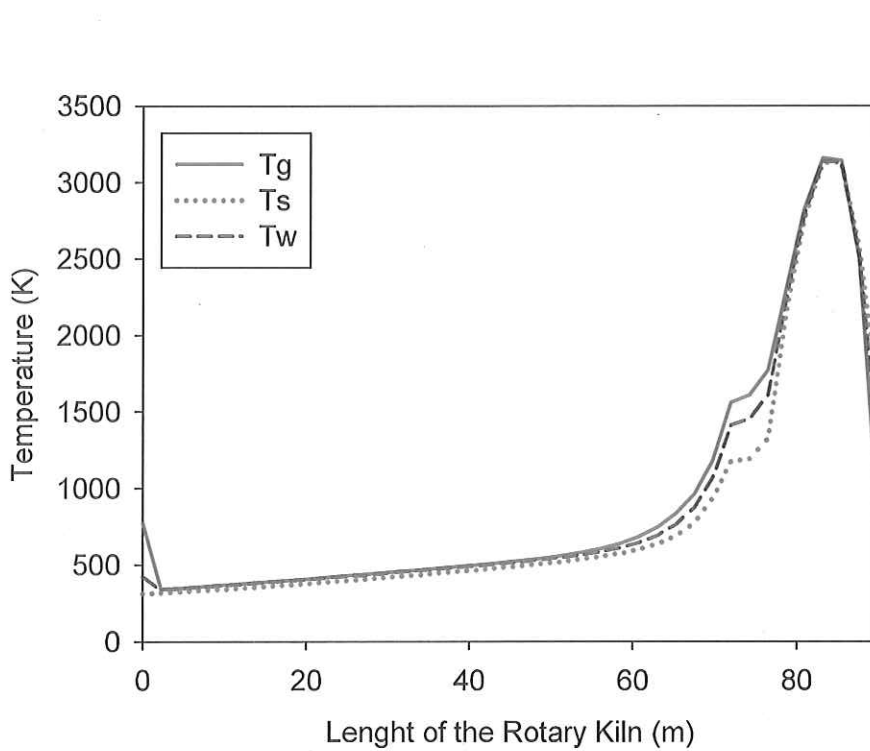


Figure 8 (a)

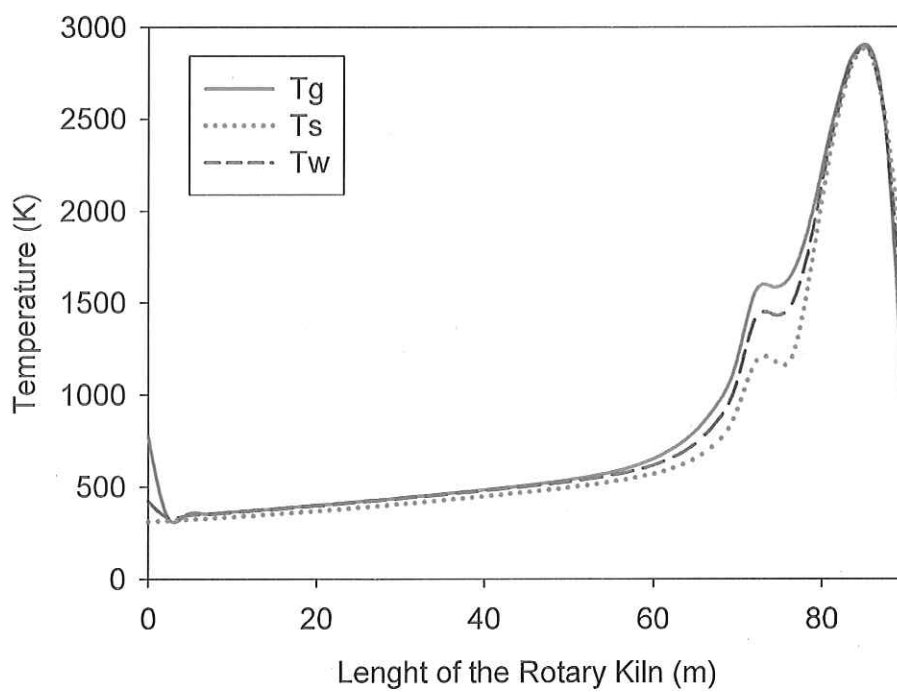


Figure 8 (b)

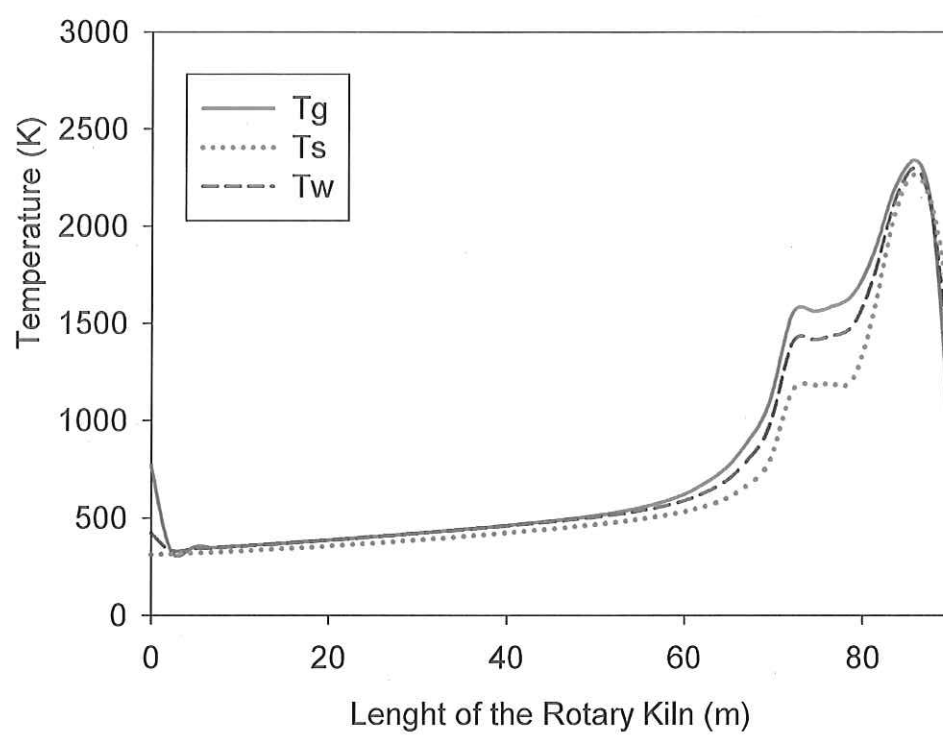


Figure 8 (c)

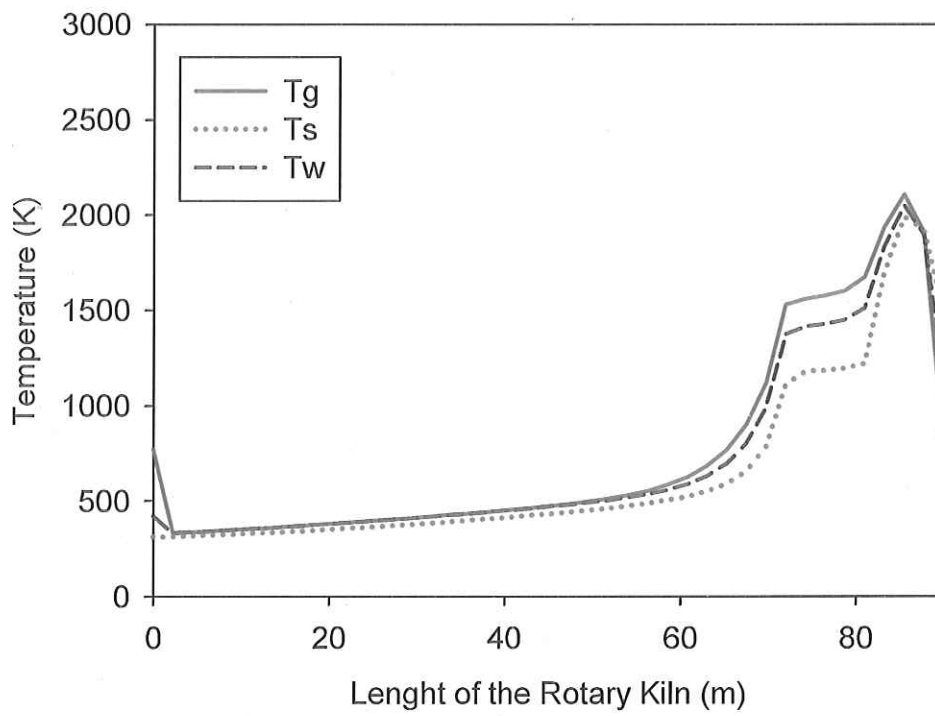


Figure 8 (d)

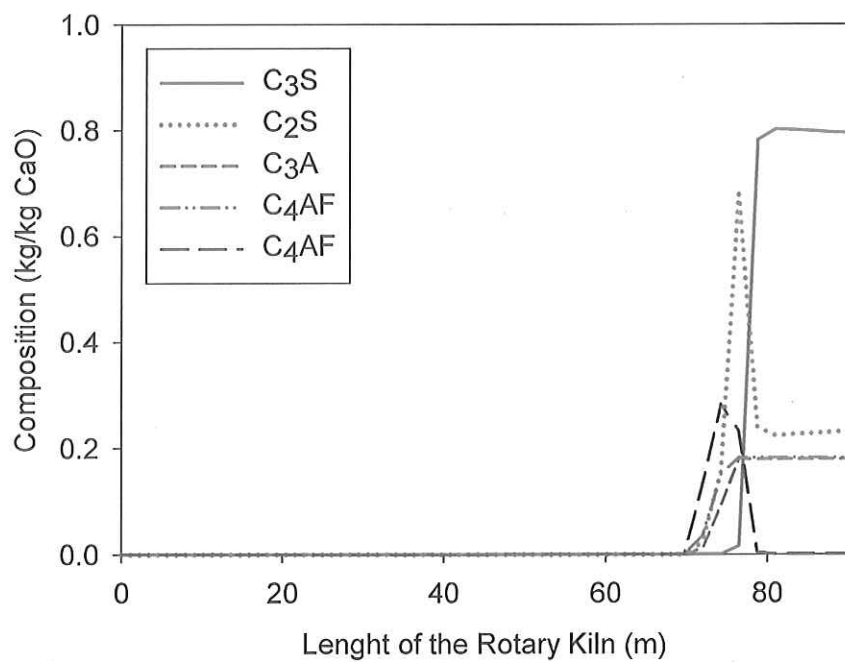


Figure 9 (a)

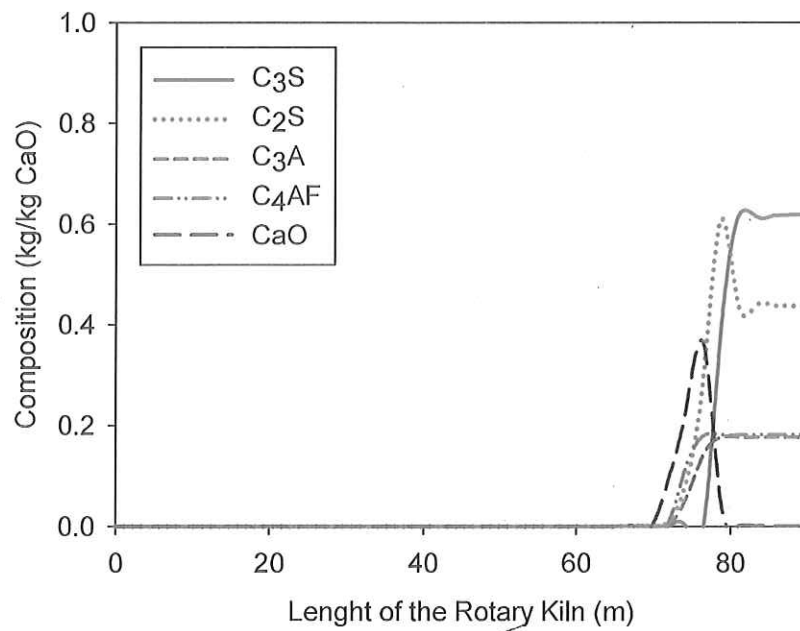


Figure 9 (b)

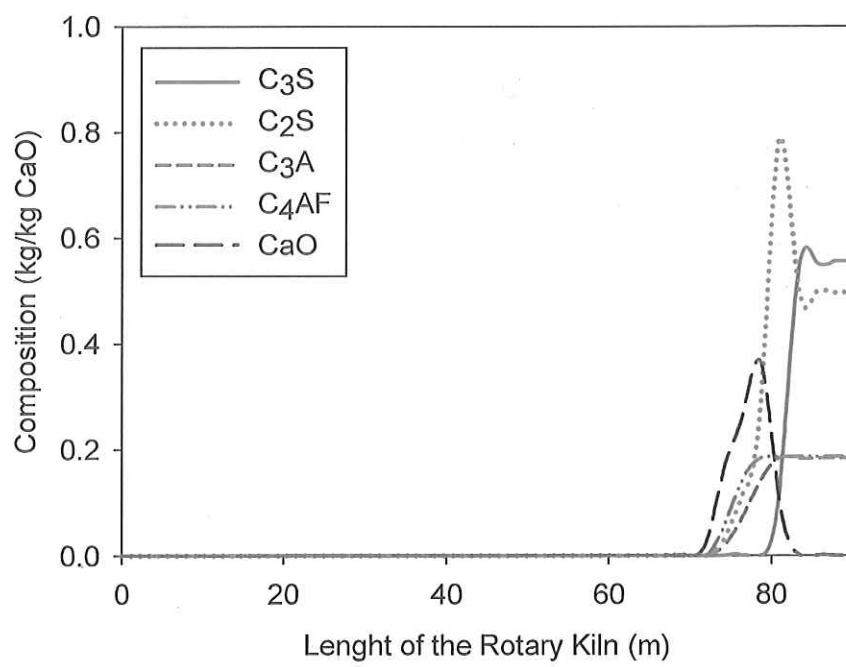


Figure 9 (c)

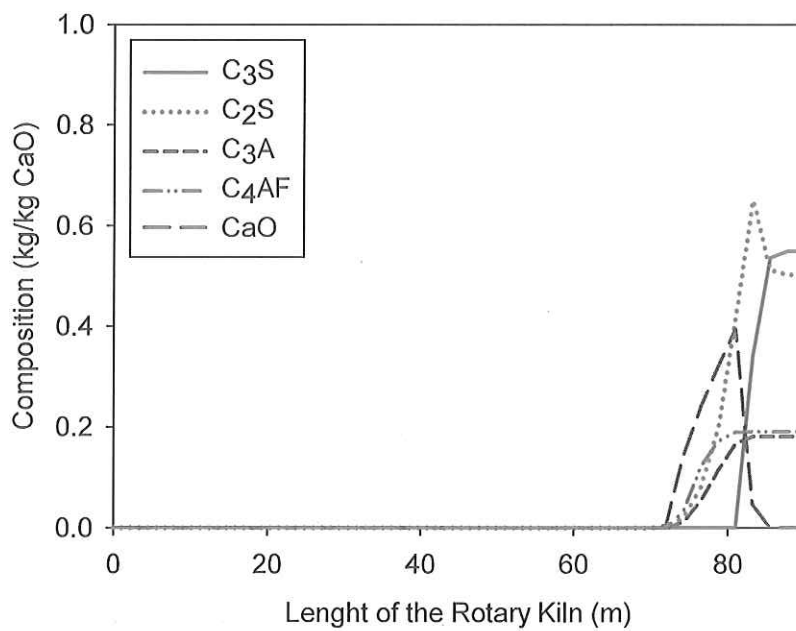


Figure 9 (d)

